Backbone Dynamics of a Two-Domain Protein: ^{15}N Relaxation Studies of the Amino-Terminal Fragment of Urokinase-Type Plasminogen Activator

Andrew P. Hansen, Andrew M. Petros, Robert P. Meadows, and Stephen W. Fesik*

Pharmaceutical Discovery Division, Abbott Laboratories, Abbott Park, Illinois 60064

Received July 22, 1994; Revised Manuscript Received October 10, 1994[⊗]

ABSTRACT: The amino-terminal fragment (ATF) of urokinase-type plasminogen activator (u-PA) is a two-domain protein which consists of a kringle and a growth factor domain (GFD). The dynamics of uniformly ^{15}N-labeled ATF was examined by measuring the longitudinal (T_1) and transverse (T_2) ^{15}N relaxation times and heteronuclear NOEs. The data were interpreted in terms of the model-independent spectral density function. The GFD was found to exhibit a high degree of anisotropy, whereas the kringle domain of ATF undergoes isotropic reorientation. This difference in anisotropy is best explained by the two domains moving independently such as differently shaped beads on a string. With the exception of the N- and C-terminal regions of the protein, the most flexible region of ATF was the seven-residue ω loop (N22−I28) of the GFD which has been implicated in the binding of u-PA to its receptor. The amides of the linker region between the domains displayed high values of the order parameter, indicating restricted motion on the picosecond time scale. This is in contrast to the flexible linker of calmodulin [Barbato et al. (1992) *Biochemistry 31*, 5269−5278], which displayed low values of S^2 and unrestricted motion in the linker region.

Multidomain proteins are involved in many diverse processes such as fibrinolysis (urokinase-type plasminogen activator, tissue-type plasminogen activator, plasmin), cell adhesion (fibronection, laminin), and signal transduction (epidermal growth factor receptor, phospholipase C, v-src protein−tyrosine kinase). Proteins with multiple binding and catalytic functions can be assembled by linking domains which possess the desired characteristics. The individual domains of multidomain proteins may interact with one another or be structurally independent and may be connected with either rigid or flexible linkers (Baron et al., 1991; Campbell & Downing, 1994). Although many three-dimensional structures have been reported for individual domains separated from the rest of the native protein, only a relatively small amount of information has appeared on the three-dimensional structure and dynamics of multidomain proteins in solution. In one study of a two-domain protein, Williams et al. (1993, 1994) determined the structure of a fibronectin fragment containing two type I modules. In their analysis, the domains were found to be rigidly linked with little or no reorientation of the interdomain linker. In another study, Barlow et al. (1993) determined the solution structure of a pair of complement modules from factor H. They observed numerous NOEs between the two domains and between the domains and linker region. From these data they inferred that the domains undergo only limited inter-modular reorientation. The preliminary secondary structure results of the fibronectin type 1 and growth factor modules from tissue-type plasminogen activator show amino acids from the two modules linked together to form a β-sheet and presumably a very rigid connection (Smith et al., 1994). In a more rigorous analysis of interdomain dynamics, Bax and co-workers applied ^{15}N relaxation measurements to the two domains of calmodulin (Barbato et al., 1992). Their analysis of the NMR data supported a "flexible tether" model for calmodulin in which the two globular domains undergo essentially isotropic reorientation.

We recently determined the solution structure of the amino-terminal fragment (ATF)[1] of urokinase-type plasminogen activator (u-PA) using heteronuclear, multidimensional NMR experiments (Hansen et al., 1994) applied to ^{15}N- and $^{15}N/^{13}C$-labeled protein obtained from mammalian cells (Hansen et al., 1992). This fragment of u-PA is composed of a kringle and growth factor domain (GFD) connected by a four-residue linker. This protein is of interest because the growth factor domain binds to the u-PA receptor, an event that is critical for tissue remodeling and the metastasis of certain tumors (Duffy, 1993). In our previous studies, we concluded that the kringle and growth factor domains are structurally independent with very little interaction between them based on the lack of interdomain NOEs and the broad signals observed in the linker region. Here we characterize the dynamics of ATF in solution from an analysis of ^{15}N relaxation data (T_1, T_2, and $^{15}N\{^1H\}$NOE) acquired on uniformly ^{15}N-labeled ATF.

MATERIALS AND METHODS

Sample Preparation. Recombinant u-PA was cloned into Sp2/0 cells and expressed in mammalian cell culture (Lo & Gillies, 1991). Uniformly ^{15}N-labeled u-PA was purified from Sp2/0 cells grown on isotopically labeled amino acids as previously described (Hansen et al., 1992) and subjected to limited autoproteolysis to generate the amino-terminal fragment (Mazar et al., 1992). The ATF NMR sample (~2 mM) was prepared in 150 μL of 25 mM sodium acetate-d_3

* To whom correspondence should be addressed.

[⊗] Abstract published in *Advance ACS Abstracts,* December 1, 1994.

[1] Abbreviations: ATF, amino-terminal fragment; u-PA, urokinase-type plasminogen activator; GFD, growth factor domain; NOE, nuclear Overhauser enhancement; BPTI, bovine pancreatic trypsin inhibitor.

0006-2960/94/0433-15418$04.50/0

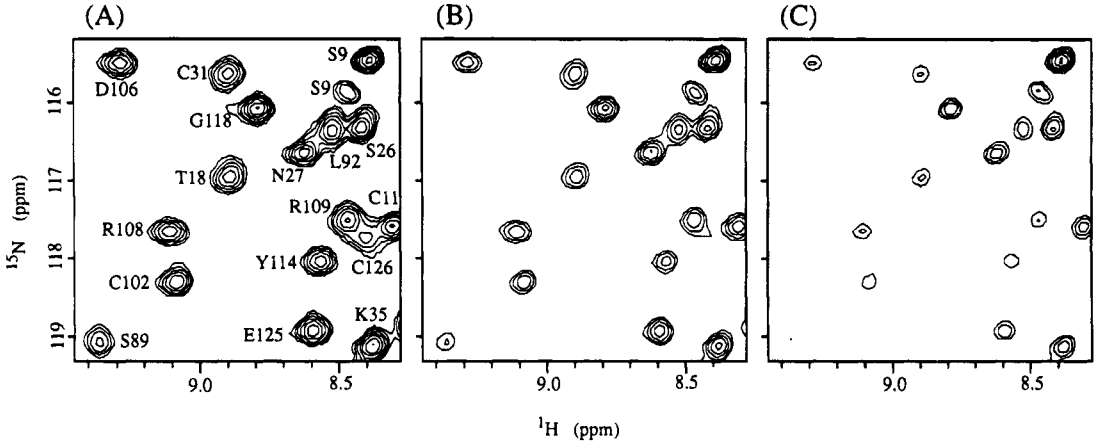

FIGURE 1: Selected region of three ^{15}N HSQC spectra used for measurement of the ^{15}N transverse relaxation times. Relaxation delays were (A) 8 ms, (B) 98 ms, and (C) 198 ms. Different conformations of P8 are responsible for the major and minor forms of S9.

buffer (pH = 4.5, 90% H_2O, 10% D_2O) and placed in a sealed microcell (Shigemi).

NMR Spectroscopy. All NMR spectra were collected at 30 °C on a Bruker AMX 500 spectrometer and were processed and analyzed using in-house written software on Silicon Graphics computers.

The spin−lattice relaxation rates, T_1, were measured using a 2D inversion recovery pulse sequence (Palmer, 1993) that was modified to include additional high-power spin locks for water suppression (Messerle et al., 1989). A total of ten 2D spectra were acquired using 256 complex points in t_1 and 2048 complex points in t_2 with eight scans per increment. The spectral widths were 1773 Hz in ω_1 (^{15}N) and 8333 Hz in ω_2 (^{1}H). T_1 relaxation delays of 5, 75, 150, 250, 400, 600, 850, 1300, 1900, and 2700 ms were used in the T_1 experiment. The relaxation delay between scans was 3.5 s.

The spin−spin relaxation rates, T_2, were measured using the pulse sequence described by Barbato et al. (1992). Ten 2D spectra were acquired with T_2 relaxation delays of 8, 16, 32, 49, 66, 98, 131, 180, 246, and 344 ms. All other acquisition parameters were identical to those in the T_1 experiments.

The error in the T_1 and T_2 measurements was estimated by performing Monte Carlo simulations based on the estimated error in the peak heights. The error in the peak heights was measured by repeating the same data point five times.

Heteronuclear NOEs were measured using the pulse sequence of Barbato et al. (1992). In these experiments one spectrum was acquired with proton saturation by applying 120° pulses at 20-ms intervals between scans and a second spectrum without saturating pulses. The acquisition of the two spectra was interleaved to minimize any differences in the spectra not due to the heteronuclear NOE. Five sets of spectra were acquired using sweep widths of 1773 and 8333 Hz over 1024 × 192 complex points in ω_1 (^{15}N) and ω_2 (^{1}H), respectively. A 6.0-s relaxation delay and eight scans per increment were used in the experiment.

RESULTS AND DISCUSSION

T_1, T_2, and NOE Data. Figure 1 depicts a selected region of the T_2 ^{15}N−^{1}H correlation spectrum of ATF acquired at three different values of the transverse relaxation delay which illustrates the quality of the data. The peak heights for each amide in this experiment and in the T_1 experiment were least squares fitted to equations with a single exponential decay. Representative fits of the data for both T_1 and T_2 are shown in Figure 2. The error in the T_1 and T_2 measurements was relatively small for most of the signals (<3%) as estimated from the Monte Carlo simulations.

The heteronuclear NOEs were more difficult to accurately measure due to the reduced sensitivity of the NOE experiment. To improve the precision and to enable an estimation of the errors, the NOE experiment was repeated five times. The average of the five NOE measurements was used in further analyses. The standard deviation of the measurements was typically less than 0.08 although peaks with short T_2s had much greater error in their NOE measurement. Figure 3 shows a graphical depiction of the measured relaxation parameters (T_1, T_2, and NOE) as a function of residue number for ATF. The T_1, T_2, and NOE values with their estimated errors are available as supplementary material.

Characterization of Overall Rotational Motion. The first step in the analysis involved the determination of the overall rotational correlation time. In order to characterize any differences between the two domains, each was treated separately. It has been shown for a spherical protein that very fast internal motions, to a first approximation, affect both T_1 and T_2 by the same amount, allowing the overall rotational correlation time to be derived from the T_1/T_2 ratio of amides not experiencing significant internal motion or chemical exchange broadening (Kay et al., 1989; Clore et al., 1990). These amides are selected by excluding peaks with a large NOE effect (NOE < 0.6) or with T_1 or T_2 values more than one standard deviation from the mean which were not excluded on the basis of the NOE. The spectral density function for isotropic tumbling is related to the correlation time, τ_r, by

$$J(\omega) = \frac{\tau_r}{1 + \omega^2 \tau_r^2} \quad (1)$$

Using this approach, rotational correlation times of 7.28 ± 0.22 ns for the growth factor domain and 7.97 ± 0.45 ns for the kringle were obtained. Although one might expect that the correlation time of the smaller GFD (40 residues) would be less than that for the kringle (85 residues), the dimensions in the longest axis of both domains are similar (Figure 4), which could account for the correlation times

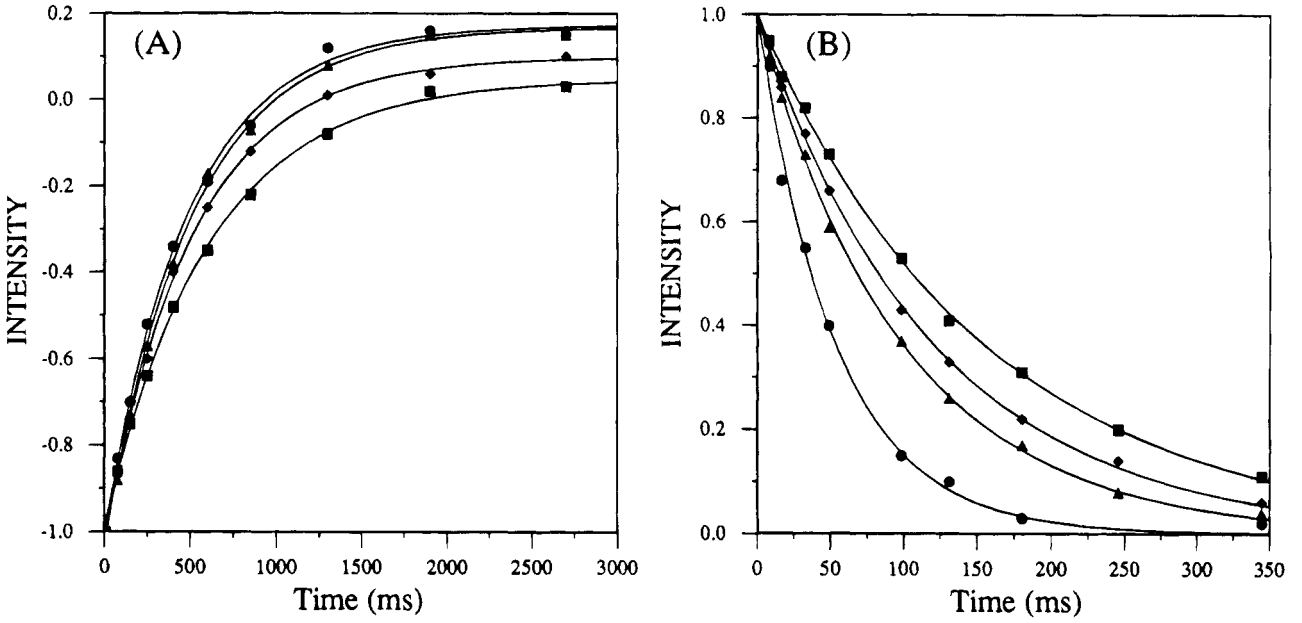

FIGURE 2: (A) T_1 and (B) T_2 relaxation curves for four residues of ATF: box = S26, diamond = K35, triangle = Y114, and circle = C126. Exponential fits are shown as solid lines.

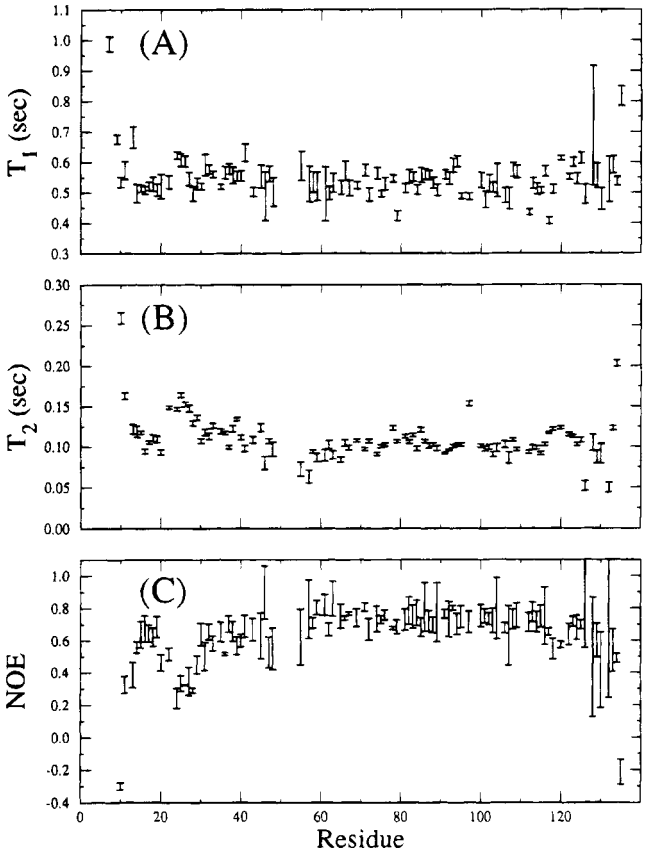

FIGURE 3: Plots of T_1 (A), T_2 (B), and NOE (C) versus residue number for ATF.

which are not statistically different at a very high confidence level. Thus, it is unclear from the calculated correlation times alone whether the two domains are reorienting independently. Indeed, it is important to consider that the shape of the GFD is far from spherical. The ratio of the three principal components of the inertial tensor is 1.00:1.15:3.77 (Figure 4A). The shape of the kringle domain is closer to a sphere with the principal components of the inertial tensor of 1.00: 1.71:1.94 (Figure 4B).

Relaxation data of molecules which do not exhibit isotropic tumbling can be fit with the model-independent spectral density function of Lipari and Szabo (1982a):

$$J(\omega) = \frac{AS^2\tau_1}{1+(\omega\tau_1)^2} + \frac{(1-A)S^2\tau_2}{1+(\omega\tau_2)^2} + \frac{A(1-S^2)\tau_{1e}}{1+(\omega\tau_{1e})^2} + \frac{(1-A)(1-S^2)\tau_{2e}}{1+(\omega\tau_{2e})^2} \quad (2)$$

where $\tau_{1e}^{-1} = \tau_1^{-1} + \tau_e^{-1}$ and $\tau_{2e}^{-1} = \tau_2^{-1} + \tau_e^{-1}$. The parameter A is a mixing function of the two correlation times τ_1 and τ_2 which describe the anisotropy of overall motion. S^2 describes the spatial restriction of the internal motion τ_e. In the special case of a cylinder freely tumbling in solution the value of the parameter A for each amide would be dependent on θ, the angle between the amide vector and the axis of the cylinder (Lipari & Szabo, 1982a).

$$A = 0.25(3\cos^2\theta - 1)^2 \quad (3)$$

In order to find the parameters which describe the overall motion for each domain (τ_1, τ_2, and A), we fit the measured T_1 and T_2 values of amides in regions of rigid secondary structure (Hansen et al., 1994) to eq 2 assuming the relaxation of these amides is not influenced by internal motion. This was done by minimizing the function

$$f(\tau_1,\tau_2,A) = \left[\frac{T_{1,\mathrm{calc}} - T_{1,\mathrm{obs}}}{T_{1,\mathrm{calc}}}\right]^2 + \left[\frac{T_{2,\mathrm{calc}} - T_{2,\mathrm{obs}}}{T_{2,\mathrm{calc}}}\right]^2 \quad (4)$$

For residues in the GFD minimization of the above equation gave correlation times, τ_1 and τ_2, of 10.45 ± 0.95 and 7.03 ± 0.19 ns. The most interesting aspect of the mixing parameter A was the dependence of this parameter on the angle θ between the amide and the principal axis of the domain (Figure 5A). For the kringle domain correlation times of 8.47 ± 0.36 and 7.76 ± 0.29 ns were found. For this domain the parameter A is mixing correlation times

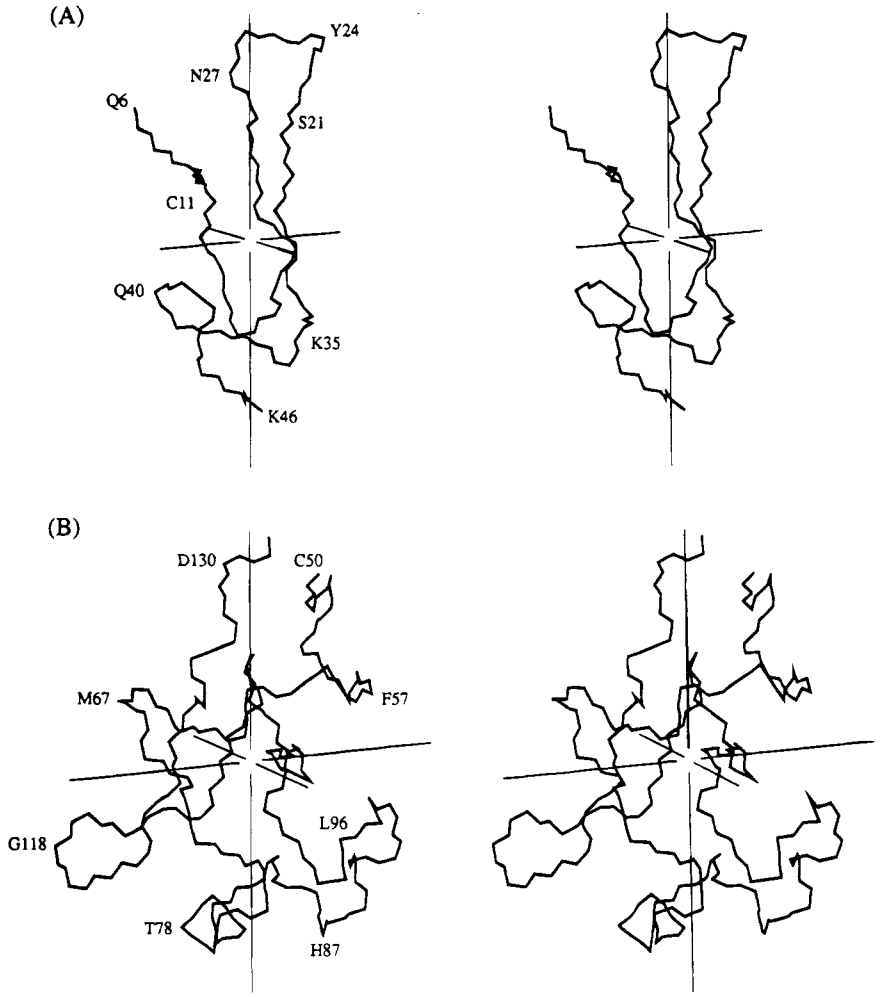

FIGURE 4: Stereo drawing of the average, minimized NMR structure of the GF domain (A) and kringle domain (B) of ATF. The three principal axes of each domain are shown as thin lines.

which are much closer in value, and therefore this parameter has less significance. When A is plotted as a function of θ, no dependence of A to the angle θ was observed for the kringle (Figure 5B). The angles to the principal axis for each domain were measured from the NMR solution structure of ATF (Hansen et al., 1994). Errors in the correlation times and A are estimated from duplicate fittings of data generated from the Monte Carlo simulations.

Although we would have liked to have more points to define the smaller angles of θ for the growth factor, most of the structured residues are in the major β-sheet which is parallel to the principal axis (Figure 4A). These amide vectors are perpendicular to the sheet and therefore the principal axis of the domain. The lack of data points on the left side is reflected in the greater error in fitting τ_1. Nevertheless, it is clear from the data, the much larger difference in τ_1 and τ_2 and the dependence of A on θ for the GFD, that the anisotropy of reorientation of the two domains is different.

The difference in anisotropy observed between the two domains can best be explained by independent reorientation of the two domains much like a sphere and a cylinder connected by a flexible string. The finding of a dependence of A on θ for the GFD suggests that its motion, although tethered to the kringle, is related to a freely tumbling cylinder. Indeed, the relaxation data for the GFD can be very well fit using the spectral density function of Woessner (1962), which describes the tumbling of a cylinder:

$$J(\omega) = A\frac{\tau_r}{1+\omega^2\tau_r^2} + B\frac{\tau_B}{1+\omega^2\tau_B^2} + C\frac{\tau_C}{1+\omega^2\tau_C^2} \quad (5)$$

with

$$\frac{1}{\tau_B} = \frac{5}{6\tau_r} + \frac{1}{6\tau_i}$$

$$\frac{1}{\tau_C} = \frac{1}{3\tau_r} + \frac{2}{3\tau_i}$$

$$A = 0.25(3\cos^2\theta - 1)^2$$

$$B = 3\sin^2\theta\cos^2\theta$$

$$C = 0.75\sin^4\theta$$

Because this spectral density function involves less adjustable parameters, the T_1/T_2 ratio was fit after amides were selected using the selection criteria of Barbato et al. (1992). A plot of the ratio T_1/T_2 vs θ is shown in Figure 6A; the line shown is a least squares fit of the data to eq 5. As expected, the kringle shows isotropic behavior when fit to this spectral density function (Figure 6B).

Two other models of overall tumbling can be excluded because they do not fit the data. A ridged connection

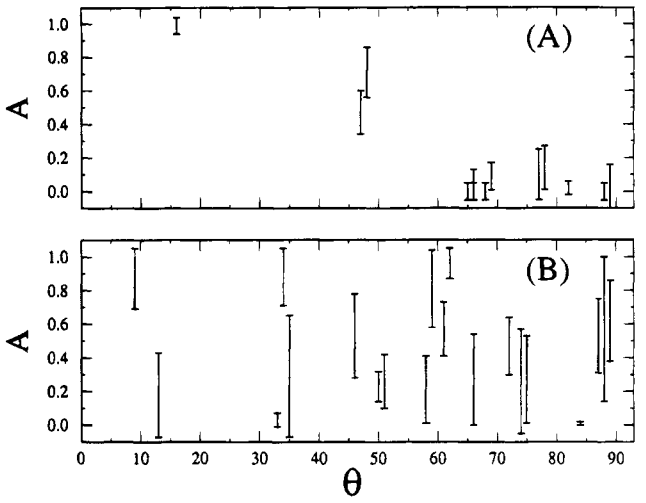

FIGURE 5: Plots of the mixing parameter A versus θ for growth factor (A) and kringle (B) domains. The parameter A is mixing correlation times of 10.45 and 7.03 ns for the growth factor and 8.47 and 7.76 ns for the kringle. θ represents the angle between the N−H vector of a particular residue and the principal axis of the domain, as described in the text.

between the two domains is unlikely because both modules would tumble together and display the same anisotropy. Another model in which the GFD and kringle are connected by a single pivot and exhibit motional properties described by wobbling in a cone can also be excluded, since A would have no dependence on θ, the angle between the axis of the cone and the N−H vector (Lipari & Szabo, 1982a).

Calculation of Model-Free Parameters. In addition to the anisotropy and relative motion of the two modules, we examined the dynamics within each domain. The internal motion of the backbone is best characterized using the "model-independent" approach of Lipari and Szabo (1982a,b). For an isotropically tumbling molecule the data are fit to the spectral density function:

$$J(\omega) = \frac{S^2\tau_r}{1+\omega^2\tau_r^2} + \frac{(1-S^2)\tau}{1+\omega^2\tau^2} \quad (6)$$

where $1/\tau = 1/\tau_r + 1/\tau_e$, S_2 describes the spatial restriction of the fast motion, and τ_e is the correlation time of this motion. For an anisotropically tumbling molecule eq 2 must be used.

The data for the kringle domain was fit using eq 6 minimizing the function

$$f(S^2) = \left[\frac{T_{1,calc} - T_{1,obs}}{T_{1,calc}}\right]^2 + \left[\frac{T_{2,calc} - T_{2,obs}}{T_{2,calc}}\right]^2 + \left[\frac{NOE_{obs} - NOE_{calc}}{2}\right]^2 \quad (7)$$

with $\tau_r = 7.97$ ns. The data for the GFD was fit using eq 2 to calculate the relaxation times of residues for which a value of A was determined. For residues which are not in rigid secondary structure no value of A has been determined. However, for residues which have internal motion the value of S^2 is not very sensitive to the overall correlation time. The data for the GFD are well described by the spectral density function for anisotropic tumbling of a cylinder (Figure 6A), with the angle θ determined from the NMR

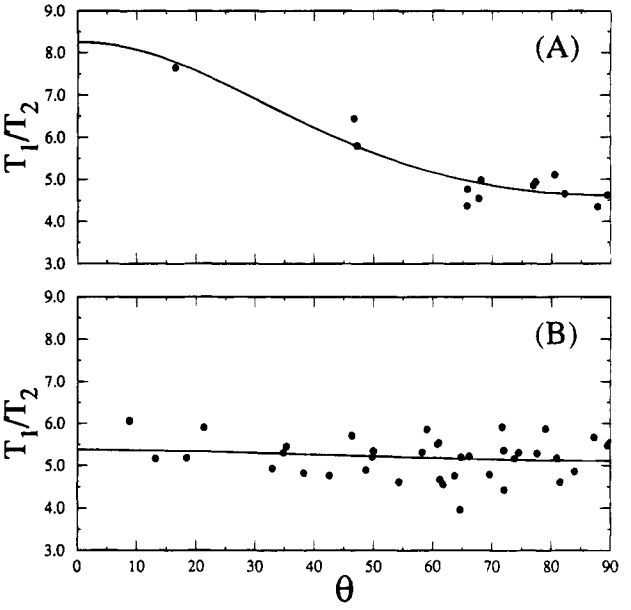

FIGURE 6: Plots of T_1/T_2 versus θ for growth factor (A) and kringle (B) domains. Shown are the least squares fits to the equation which describes anisotropic tumbling of a cylinder.

structure. Equation 5 can be expanded to include internal motion:

$$J(\omega) = S^2\left[A\frac{\tau_r}{1+\omega^2\tau_r^2} + B\frac{\tau_B}{1+\omega^2\tau_B^2} + C\frac{\tau_C}{1+\omega^2\tau_C^2}\right] + (1-S^2)\left[\frac{\tau}{1+\omega^2\tau^2}\right] \quad (8)$$

with all parameters retaining their previously defined meaning. This equation allows a value of S^2 to be determined for all residues. To check the magnitude of the errors possible using the above equation, the data for the GFD were fit to the isotropic spectral density function using correlation times of 7.0 and 10.5 ns. The values of S^2 from these two fits were within the estimated error for most of the residues. In general, the fit using 10.5 ns introduced a systematic error resulting in values of S^2 slightly lower than the reported values, and the fit using 7.0 ns gave values slightly higher. In both fits the trends in the order parameter were retained. The order parameter determined for each amide of [U-^{15}N]-ATF is displayed graphically in Figure 7A.

The above approach can also be used to obtain values of τ_e, the correlation time of internal motion. However, if this motion is in the picosecond range, the value of τ_e has very little effect on the spectral density as S^2 becomes large. The insensitivity of the calculated relaxation values to large changes in τ_e can lead to errors of over 100% in τ_e from 5% errors in measurement of the relaxation rates or NOE (Palmer et al., 1991). In general, the values of τ_e reflect the same trends found in S^2, which can be much more reliably fit. Therefore, we only report the values of S^2.

For residues undergoing conformational averaging or exchange comparable to the chemical shift difference of the conformers, the value of T_2 will be shortened. Fitting these residues to eq 6 will result in a large error in the second term of eq 7. For these residues the fit can be improved by including a chemical exchange term in the T_2 relaxation rate. The magnitude of the increase in line width due to chemical exchange (R_{ex}) is plotted in Figure 7B. The values of A, S^2,

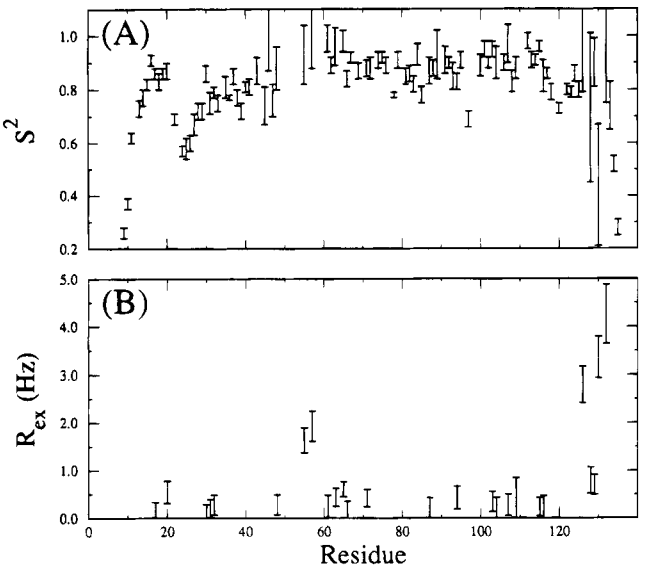

FIGURE 7: Plots of S^2 (A) and line width of R_{ex} (B) versus residue for ATF.

and R_{ex} along with their estimated errors are available as supplementary material.

The largest structural element of the GFD is a two-strand β-sheet formed by residues T18−S21 and H29−N32. These residues exhibit the highest order parameters in the domain. The two strands of this β-sheet are joined by the most flexible region of the domain (excluding the unstructured N-terminal region)—a seven-residue ω loop (N22−I28). Order parameters in this loop region drop to less than 0.6 compared to values of over 0.8 in the β-sheet (Figure 6A). It is interesting to note that the residues of this loop region have been implicated in binding of u-PA to the u-PA receptor (Appella et al., 1987), suggesting that in the absence of the receptor this loop undergoes a large amount of internal motion. Upon binding to the u-PA receptor, this loop may become much less mobile. A recent ^{15}N-relaxation study by Chen et al. (1994) has also found very low order parameters in the nine-residue loop between two strands of a β-sheet in the snake venom protein echistatin, which contains the RGD sequence responsible for binding to integrin receptors.

In general, the order parameters for the GFD are slightly lower than most well-structured domains. A possible explanation is that this domain lacks a hydrophobic core that holds the individual elements of secondary structure in a well-defined position. This internal motion was reflected in the slightly higher rmsd found between calculated structures of this domain (Hansen et al., 1994).

The kringle domain shows more overall order as reflected in the higher values of S^2. Almost all the amides of the kringle have order parameters greater than 0.80, and most amides in the β-sheet or α-helices had order parameters greater than 0.90. The exceptions include the turn between the two strands of the largest β-sheet (V117−K120), in which order parameters dropped to under 0.75, and G97, which forms part of a loop region between a short α-helix and a short β-sheet.

Although the kringle showed very restricted fast internal motion, several regions exhibited motion on the slower time scale of conformational averaging. The regions with large values of R_{ex} were all near cysteine residues. The highest values of R_{ex} were near both sides of the C50−C131 disulfide bond. All of the amides near these cysteines had very large values of R_{ex} or were not assigned due to very broad line widths. C126 also exhibited a large value of R_{ex}, although adjacent residues were not affected (see E125 and C126 in Figure 1). Increased transverse relaxation rates have been previously noted for residues near C14 and C38 of bovine pancreatic trypsin inhibitor (BPTI) which are connected by a disulfide bond. Wüthrich and co-workers have recently shown that this broadening is caused by chemical exchange between different conformations of the disulfide bond (Otting et al., 1993; Szyperski et al., 1993).

Residues in the linker region for which assignments could be made exhibited short T_2s and average heteronuclear NOEs, indicating little motion on the picosecond time scale. This behavior is in sharp contrast to the flexible tether region found by Barbato et al. (1992) for calmodulin. The amides of the flexible region in the central α-helix which connects the domains of calmodulin have long T_1 and T_2 values and large NOEs, indicative of fast unrestricted motions of the backbone.

CONCLUSIONS

Previous studies have suggested that the GFD and kringle domain are structurally independent (Bogusky et al., 1989; Oswald et al., 1989; Nowak et al., 1983; Novokhatny et al., 1992, 1993; Hansen et al., 1994). The difference in anisotropy between the two domains found here is best explained by independent motion of the two connected modules. Trends in the order parameters of internal motion were consistent with trends observed in previous heteronuclear relaxation studies of proteins in solution. For example, amides in elements of regular secondary structure exhibit the highest order parameters with less restricted motion in loops and turns. The most flexible loop (N22−I28) has been implicated as the binding site of the u-PA receptor.

Very few structural studies of multidomain proteins in solution have been reported (Barlow et al., 1993; Smith et al., 1994; Williams et al., 1994; Hansen et al., 1994). The characteristics of the linker region in these proteins, inferred from NOEs, have varied widely from interlocking strands of β-sheet to a flexible tether. Heteronuclear relaxation measurements to characterize the dynamics of multidomain proteins have only been previously applied to the domains of calmodulin (Barbato et al., 1992). Although both calmodulin and ATF have a flexible linker, the time scale of motion in the linker region was very different in the two proteins. Recent developments in heteronuclear NMR allow for detailed structural and dynamic characterization of large multidomain proteins. It will be of interest to study other multidomain proteins to determine how domain−domain interactions and mobility correlate to biological function.

ACKNOWLEDGMENT

We thank Terry Pederson for growth of Sp2/0 cells, Andrew Mazar for purification of ATF, Jack Henkin for encouragement and support, and Leon O. Morgan for helpful discussions.

SUPPLEMENTARY MATERIAL AVAILABLE

Two tables with the measured T_1, T_2, and NOE values along with their estimated errors and the fitted values of S^2

and R_{ex} (10 pages). Ordering information is given on any current masthead page.

REFERENCES

Appella, E., Robinson, E., Ulrich, S., Stoppelli, M., Corti, A., Cassani, G., & Blasi, F. (1987) *J. Biol. Chem. 262*, 4437−4440.

Barbato, G., Ikura, M., Kay, L. E., Pastor, R. W., & Bax, A. (1992) *Biochemistry 31*, 5269−5278.

Barlow, P. N., Steinkasserer, A., Norman, D. G., Kieffer, B., Wiles, A. P., Sim, R. B., & Campbell, I. D. (1993) *J. Mol. Biol. 232*, 268−284.

Baron, M., Norman, D. G., & Campbell, I. D. (1991) *Trends Biochem. Sci. 16*, 13−17.

Bogusky, M. J., Dobson, C. M., & Smith, R. A. G. (1989) *Biochemistry 28*, 6728−6735.

Campbell, I. D., & Downing, A. K. (1994) *Trends Biotechnol. 12*, 168−172.

Chen, Y., Suri, A. K., Kominos, D., Sanyal, G., Naylor, A. M., Pitzenberger, S. M., Garsky, V. M., Levy, R. M., & Baum, J. (1994) *J. Biomol. NMR 4*, 307−324.

Clore, G. M., Driscoll, P. C., Wingfield, P. T., & Gronenborn, A. M. (1990) *Biochemistry 29*, 7387−7401.

Duffy, M. J. (1993) *Fibrinolysis 7*, 295−302.

Hansen, A. P., Petros, A. M., Mazar, A. P., Pederson, T. M., Rueter, A., & Fesik, S. W. (1992) *Biochemistry 31*, 12713−12718.

Hansen, A. P., Petros, A. M., Meadows, R. P., Nettesheim, D. G., Mazar, A. P., Olejniczak, E. T., Xu, R. X., Pederson, T. M., Henkin, J., & Fesik, S. W. (1994) *Biochemistry 33*, 4847−4864.

Kay, L. E., Torchia, D. A., & Bax, A. (1989) *Biochemistry 28*, 8972−8979.

Lipari, G., & Szabo, A. (1982a) *J. Am. Chem. Soc. 104*, 4546−4559.

Lipari, G., & Szabo, A. (1982b) *J. Am. Chem. Soc. 104*, 4559−4570.

Lo, K.-M., & Gillies, S. D. (1991) *Biochim. Biophys. Acta 1088*, 217−224.

Mazar, A. P., Buko, A., Petros, A. M., Barnathan, E. S., & Henkin, J. (1992) *Fibrinolysis 6* (Suppl. 1), 49−55.

Messerle, B. A., Wider, G., Otting, G., Weber, C., & Wüthrich, K. (1989) *J. Magn. Reson. 85*, 608−613.

Novokhatny, V., Medved, L., Mazar, A., Marcotte, P., Henkin, J., & Ingham, K. (1992) *J. Biol. Chem. 267*, 3878−3885.

Novokhatny, V. V., Medved, L. V., Mazar, A., & Ingham, K. C. (1993) *J. Biol. Chem. 268*, 17211−17218.

Nowak, U. K., Li, X., Teuten, A. J., Smith, R. A. G., & Dobson, C. M. (1993) *Biochemistry 32*, 298−309.

Oswald, R. E., Bogusky, M. J., Bamberger, M., Smith, R. A. G., & Dobson, C. M. (1989) *Nature 337*, 579−582.

Otting, G., Liepinsh, E., & Wüthrich, K. (1993) *Biochemistry 32*, 3571−3582.

Palmer, A. G., III (1993) *Curr. Opin. Biotechnol. 4*, 385−391.

Palmer, A. G., III, Rance, M., & Wright, P. E. (1991) *J. Am. Chem. Soc. 113*, 4371−4380.

Smith, B. O., Downing, A. K., Dudgeon, T. J., Cunningham, M., Driscoll, P. C., & Campbell, I. D. (1994) *Biochemistry 33*, 2422−2429.

Szyperski, T., Luginbühl, P., Otting, G., Güntert, P., & Wüthrich, K. (1993) *J. Biomol. NMR 3*, 151−164.

Williams, M. M., Phan, I., Baron, M., Driscoll, P. C., & Campbell, I. D. (1993) *Biochemistry 32*, 7388−7395.

Williams, M. M., Phan, I., Harvey, T. S., Rostagno, A., Gold, L. I., & Campbell, I. D. (1994) *J. Mol. Biol. 235*, 1302−1311.

Woessner, D. E. (1962) *J. Chem. Phys. 37*, 647−654.